Copyright Notice

Institute of Communication Networks and Computer Engineering
University of Stuttgart
Pfaffenwaldring 47, D-70569 Stuttgart, Germany
Phone: ++49-711-685-68026, Fax: ++49-711-685-67983
email: mail@ikr.uni-stuttgart.de, http://www.ikr.uni-stuttgart.de

A Graph-Based Scheme for Distributed Interference Coordination in Cellular OFDMA Networks

Marc C. Necker
Institute of Communication Networks and Computer Engineering, University of Stuttgart
Pfaffenwaldring 47, D-70569 Stuttgart, Germany
Email: marc.necker@ikr.uni-stuttgart.de

***Abstract*— Wireless systems based on Orthogonal Frequency Division Multiple Access (OFDMA) multiplex different users in time and frequency. One of the main problems in OFDMA-systems is the inter-cell interference. A promising approach to solve this problem is interference coordination (IFCO). In this paper, we present a novel distributed IFCO scheme, where a central coordinator communicates coordination information in regular time intervals. This information is the basis for a local inner optimization in every basestation. The proposed scheme achieves an increase of more than 100% with respect to the cell edge throughput, and a gain of about 30% in the aggregate spectral efficiency compared to a reuse 3 system.**

I. Introduction

OFDMA has become the basis for several emerging broadband cellular networks, such as 802.16e (WiMAX), or 3GPP Long Term Evolution (LTE). In an OFDMA-system, many users are multiplexed in time and frequency on the basis of the underlying OFDM transmission system. A major problem of OFDMA in a reuse 1 scenario is the inter-cellular interference which occurs if neighboring basestations transmit on the same resources. A promising approach to solve this problem is interference coordination (IFCO), where transmissions of neighboring basestations are coordinated to minimize the interference.

IFCO has been an active topic especially in the 3GPP standardization body. Most activities have focused on local schemes operating on local state information in every basestation. These schemes are often based on power regulation [1] or Fractional Frequency Reuse (FFR) [2]. A number of FFR-based schemes was compared in [3] and [4]. Another local scheme was proposed by Xiao et al. in [5]. Kiani et al. propose a distributed scheme based on local measurements [6]. The authors measure the increase in the overall network capacity, but do not consider fairness issues, such as the throughput at the cell edge. In [7], Li et al. propose a distributed scheme by formulating a local and a global optimization problem, thus being able to include global state information in the coordination process. They consider only one strongest interferer and also do not consider fairness issues. However, fairness is crucial, especially since it is easy to sacrifice cell edge throughput in favor of overall network throughput [8]. All proposed local schemes have difficulties with this issue. In the following, we therefore explore a distributed scheme based on periodically distributed global coordination information, and we explicitly consider the performance at the cell edge compared to the aggregate throughput as a fairness metric.

In [9], we developed Coordinated FFR, where a central coordinator distributes coordination information in intervals in the order of seconds. The scheme efficiently utilizes beamforming antennas and achieves a good cell edge performance. In this paper, we present a novel distributed interference coordination scheme, in which a central coordinator solves an outer optimization problem based on global information collected from the basestations, and the basestations solve a local inner optimization problem based on local state information. The communication with the central coordinator can be in intervals in the order of seconds. The performance of the proposed scheme is significantly increased compared to Coordinated FFR and pushed further towards the (theoretical) performance of a globally coordinated system. In particular, the presented scheme outperforms a frequency reuse 3 sytem by more than 100% with respect to the cell edge throughput while increasing the aggregate throughput performance by more than 30%.

This paper is structured as follows. In section II we give an overview of the considered 802.16e system. Section III reviews the global interference coordination scheme from [10]. Subsequently, section IV and V introduce the new interference coordination scheme, and section VI evaluates its performance. Finally, section VII concludes the paper.

II. Overview of Cellular 802.16e System Model

As an example of an OFDMA network, we consider a cellular 802.16e-system [11]. In 802.16e, each MAC-frame is subdivided into an uplink and a downlink subframe. Both subframes are further divided into zones, allowing for different operational modes. In this paper, we focus on the Adaptive Modulation and Coding (AMC) zone in the downlink subframe. In particular, we consider the AMC 2x3 mode, which defines subchannels of 16 data subcarriers by 3 OFDM-symbols.

Our scenario consists of a hexagonal cell layout comprising 19 basestations at a distance of $d_{\mathrm{BS}} = 1400$ m with 120° cell sectors. The scenario is simulated with wrap-around, making all cells equal with no distinct center cell. All cells were assumed to be synchronized on a frame level. Every basestation has 3 transceivers, each serving one cell sector. The transceivers are equipped with linear array beamforming antennas with 4 elements and gain patterns according to [10]. They can be steered towards each terminal with an accuracy of 1° degree, and all terminals can be tracked ideally.

III. Graph-Based Interference Coordination

In [10], we introduced a scheme for global interference coordination based on an interference graph. In the interference graph, the vertices represent the mobile terminals, and

the edges represent critical interference relations between the mobile terminals. The interference graph is created every MAC frame. Subsequently, a global omniscient device assigns resources to the mobile terminals while obeying the restrictions imposed by the interference graph (see [8] for details). In the following section III-A, we briefly rehearse the creation of the interference graph, since it is the basis for all further studies.

A. Creation of interference graph

The interference graph is constructed by evaluating the interference that a transmission to one mobile terminal causes to any other terminal. For each terminal, we first calculate the total interference and then block the largest interferers from using the same set of resources by establishing a relation in the interference graph. This is done such that a desired minimum SIR D_S is achieved.

Let m_k and m_l be two mobile terminals in different cell sectors, as illustrated in Fig. 1. tr_i denotes the transceiver serving cell sector i. p_{ik} describes the path loss from transceiver tr_i to terminal m_k, including shadowing. We further introduce the function $G_i(l,k)$. It describes the gain of the sector i beamforming antenna towards terminal m_k when the array is directed towards terminal m_l.

In a first step, we calculate the interference I_{kl} which a transmission to mobile m_l in sector i would cause to mobile m_k in sector j, where $i \neq j$:

$$I_{kl} = p_{ik} G_i(l,k) P_l \quad , \tag{1}$$

where P_l is the transmission power of transceiver i towards terminal m_l. For each terminal m_k, we collect all interference relations in the set W_k:

$$W_k = \{ I_{kl}, \ \forall \ l \neq k, |c_l - c_k| \leq d_{ic} \} \quad . \tag{2}$$

c_l are the geographic coordinates of the transceiver serving the cell sector where terminal m_l is located in. The coordination diameter d_{ic} then denotes the maximum distance which two basestations may have in order to still be coordinated.

We then keep removing the largest interferer from W_k until the worst-case SIR for terminal m_k rises above a given desired SIR threshold D_S:

$$\text{SIR}_k = \frac{S_k}{\sum\limits_{I_{kl} \in W_k} I_{kl}} \geq D_S \quad . \tag{3}$$

S_k is the received signal strength of terminal m_k if it is served:

$$S_k = p_{jk} G_j(k,k) P_k \quad . \tag{4}$$

Let $e_{kl} \in \{0,1\}$ be the elements of the interference graph's adjacency matrix E, i.e., the edges of the interference graph, which indicate an interference relation between terminals m_k and m_l if $e_{kl} = 1$:

$$e_{kl} = \begin{cases} 0 & \text{if } I_{kl} \in W_k \wedge I_{lk} \in W_l \wedge tr(m_l) \neq tr(m_k) \\ 1 & \text{otherwise} \end{cases} , \tag{5}$$

where $tr(m_l)$ denotes the transceiver serving mobile m_l. Equation (5) sets an interference relation e_{kl} if terminal m_k causes interference to terminal m_l, or vice versa. This results in a non-directional interference graph, i.e., E is symmetric. Finally, all mobile terminals within a cell sector must be assigned disjoint resources. Hence, $e_{kl} = 1$ if m_k and m_l belong to the same cell sector, i.e., $tr(m_l) = tr(m_k)$.

B. Resource assignment by graph coloring

After the interference graph has been created, resources need to be assigned to the mobile terminals such that no two mobile terminals are assigned the same resources if they are connected in the graph. This is equal to coloring the graph if the resources correspond to colors [8]. Resources may be mapped to colors $c_{k,i} \in \mathbf{C}$ as shown in Fig. 2. Every AMC zone is subdivided into a certain number N_p of resource partitions. Several AMC zones in subsequent MAC frames form one *virtual frame* such that the total number of resource partitions in the virtual frame corresponds to the number of required colors during the coloring process (precisely: to the next larger multiple of N_p). This allows use of standard graph coloring algorithms for the resource assignment (see [8]).

C. Performance enhancement by graph separation

Two parameters affect the properties of the interference graph, such as the vertex degree or the chromatic number. First, an increase of the desired SIR D_S will lead to a more densely meshed graph, thus increasing the vertex degree and the chromatic number. Second, an increase of the coordination diameter d_{ic} will have a similar effect. In general, an increase of the chromatic number leads to a lower resource utilization [10]. At the same time, a higher D_S or d_{ic} will enhance the SIR. Both of these effects lead to a tradeoff and a maximum of the system performance for a particular parameter choice.

If $d_{ic} = 0$, then D_S may be chosen relatively high while maintaining a low vertex degree and chromatic number. This will allow for a high aggregate throughput. If D_S is chosen small, then d_{ic} may be set to a larger value while maitaining an acceptable vertex degree and chromatic number. This will ensure a good performance at the cell edge. It is therefore beneficial to create two separate interference graphs with the just described parameter choices and subsequently merge them to a single graph (see [9]). This introduces two separate desired minimum SIR parameters $D_{S,i}$ and $D_{S,o}$, one for the inner graph with $d_{ic} = 0$, and one for the outer graph with $d_{ic} \geq 1$.

IV. Distributed Interference Coordination

In this section, we present a novel scheme for distributed interference coordination. The scheme uses a central coordinator which is responsible for the coordination of neighboring

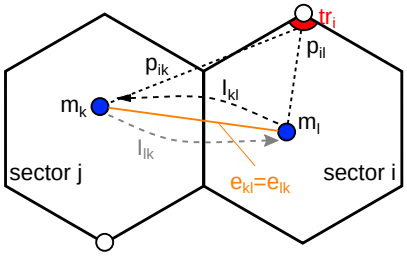

Fig. 1: Creation of interference graph

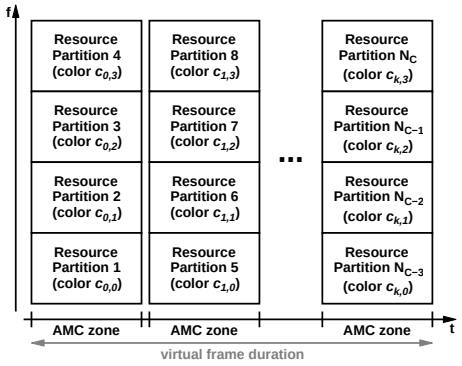

Fig. 2: Resource partitioning with $N_p = 4$

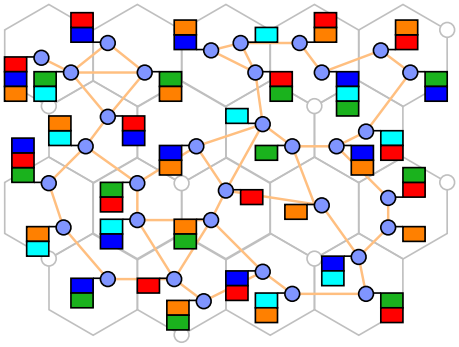

Fig. 3: Graph coloring of outer optimization problem. Flags indicate assigned colors.

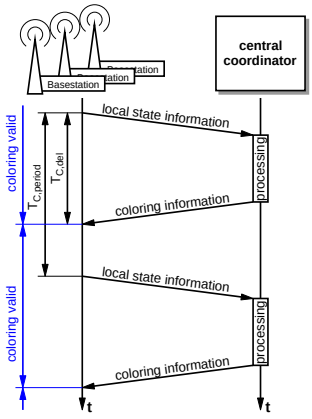

Fig. 4: Timing diagram

base-stations based on a global interference graph. At the same time, every basestation creates a local interference graph with $d_{ic} = 0$ to coordinate the transmissions in its three sectors. In contrast to Coordinated FFR [9], the newly proposed scheme takes a formal approach by formulating an *inner* optimization problem, which needs to be solved by every basestation. This inner optimization problem is subject to constraints delivered by the *outer* optimization problem, which is solved in the central coordinator. Since the communication with the coordinator may take place in time intervals in the order of seconds, this is a true distributed scheme with a practical application.

A. Outer Optimization Problem

The outer optimization problem is solved by the central coordinator based on an interference graph with $d_{ic} \geq 1$. This interference graph is created just like the interference graph required for the coordinated FFR in [9]. This graph creation may be based on measurements obtained from the mobile terminals and collected by the central coordinator and is out of the scope of this paper.

The goal of the outer optimization problem is to find a set of colors $\mathbf{C}_i \subseteq \mathbf{C}$ (i.e., a set of resource partitions) for every mobile terminal m_i such that there is no conflict between any combination of colors in the sets. This problem is known as *fractional graph coloring*. An example for a possible coloring is shown in Fig. 3. Like regular graph coloring, fractional graph coloring is an NP hard problem. Here, we take the following approach to solve the outer optimization problem. We first color the graph by means of the simple sub-optimal coloring heuristic Dsatur [12]. Next, we traverse all mobile terminals in a random order and assign a second color to every mobile terminal where possible. We repeat this step until no more extra colors can be assigned to any mobile terminal.

B. Inner Optimization Problem

The goal of the inner optimization problem is to assign every mobile terminal to one or more resource partitions $c_{k,l}$ of the respective cell sector. This means that every mobile terminal is assigned a set of colors $\mathbf{R}_i \subseteq \mathbf{C}_i$ on which it is served. That is, $\mathbf{R}_i$ must be chosen from the color set $\mathbf{C}_i$ assigned to mobile terminal m_i by the coordinator. To formulate the optimization problem we introduce for every mobile m_i the matrix $(x_{i,k,l})$, which describes the resource allocation for a particular cell sector:

$$x_{i,k,l} = \begin{cases} 1 & \text{if mobile } m_i \text{ is served in resource } c_{k,l} \\ 0 & \text{if mobile } m_i \text{ is not served in resource } c_{k,l} \end{cases} . \tag{6}$$

This means that $\mathbf{R}_i$ can be defined as

$$\mathbf{R}_i = \{c_{k,l} \mid x_{i,k,l} = 1\} \quad . \tag{7}$$

We further define a utility u_i for every mobile terminal m_i. u_i is a real number and denotes the utility if the mobile terminal is scheduled in a MAC frame. It is therefore better to schedule mobile terminals with a higher utility u_i more often.

Considering the utility u_i, the objective function of the inner optimization problem for basestation b then is

$$\max \left(\sum_{m_i \in M_b} \sum_k \sum_l u_i x_{i,k,l} \right) \quad , \tag{8}$$

where M_b contains all mobiles m_i which are served by any of the three transceivers of basestation b. Eq. (8) maximizes the utility sum for the respective basestation. Note that eq. (8) maximizes the resource allocation for one virtual frame. Hence, the resource allocation problem has to be solved at the beginning of every virtual frame.

The inner optimization problem is subject to a number of constraints.

1) Every mobile m_i has to be served using one of the colors in $\mathbf{C}_i$ assigned by the central coordinator:

$$\forall \{x_{i,k,l} \mid x_{i,k,l} = 1\} : \; c_{k,l} \in \mathbf{C}_i \quad . \tag{9}$$

2) Every mobile terminal has to be served at least once in every virtual frame:

$$\forall i : \sum_k \sum_l x_{i,k,l} \geq 1 \quad . \tag{10}$$

3) Every mobile terminal must not be served more than once per MAC frame:

$$\forall i \forall k : \sum_l x_{i,k,l} \leq 1 \quad . \tag{11}$$

4) The constraints of the local interference graph have to

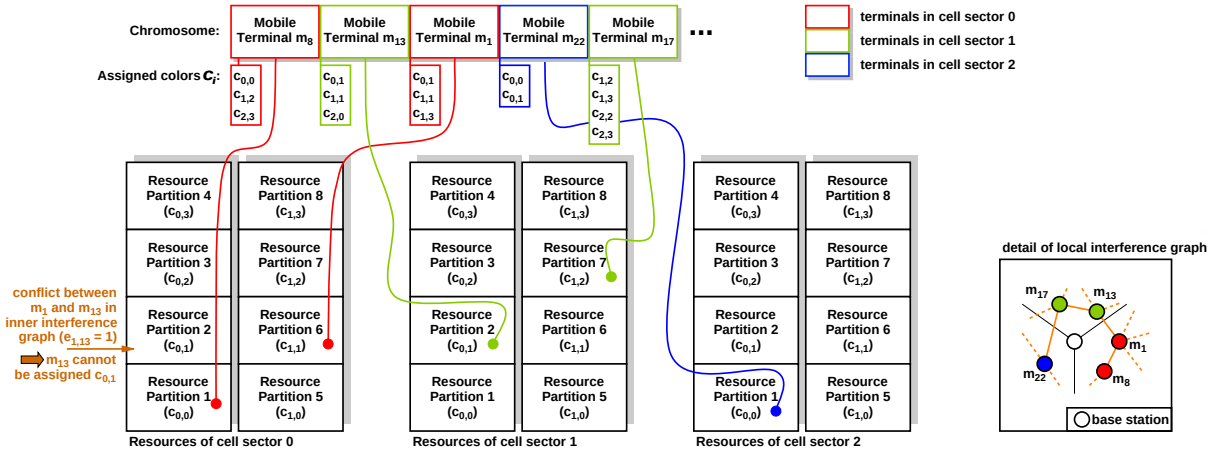

Fig. 5: Representation of genome as list of terminals and sequential assignment of terminals in list to resources in cell sectors. This example contains a conflict in the inner graph between mobile m_1 and m_{13} (i.e., $e_{1,13} = 1$), which is why m_1 cannot be assigned $c_{0,1}$.

be met:

$$\forall \{(i,j) \mid e_{ij} = 1\} : \mathbf{R}_i \cap \mathbf{R}_j = \varnothing \qquad (12)$$

The optimization problem formulated by equations (8)–(12) is a binary integer linear program (BILP), which is NP-hard to solve. BILPs can be treated by standard optimization packages for integer linear programs (ILPs), but represent a particularly difficult class of ILPs. In section V, we will efficiently treat this problem by means of genetic algorithms.

C. System Architecture

The system architecture comprises a central coordinator responsible for creating the interference graph and solving the outer optimization problem. All basestations communicate the necessary data to the central coordinator, as shown in the timing diagram in Fig. 4. The set of colors is then communicated from the central coordinator to the basestations, which periodically solve the inner optimization problem. Communication with the central coordinator takes place with an update period $t_{C,up}$. The delay $t_{C,delay}$ contains all signalling delays, processing delays and synchronization delays.

V. Solution of Inner Optimization Problem with Genetic Algorithms

This section discusses the possibility of solving the inner optimization problem by means of genetic algorithms. First, section V-A gives a short introduction to genetic algorithms. In section V-B, we describe the modeling approach for the inner optimization problem. Finally, section V-C describes the applied genetic operators.

A. Introduction to genetic algorithms

Genetic algorithms are a well known heuristic approach to solve complex optimization problems. They are based on generations of solutions. Every generation contains a number $|P|$ of possible solutions to the optimization problem, which are called *genomes*. Every genome is evaluated and assigned a *fitness* value. This fitness value is highly problem specific and indicates how "good" the solution is.

Every generation serves as the basis for a new generation. To generate the genomes of the new generation, the genomes of the old generation are copied, mutated, or combined. These operations are performed by genetic operators, namely a copy operator, a mutator, and a crossover operator.

B. Genetic representation and modeling

The representation of a solution is problem-specific and often not obvious. The challenge lies in finding a compact representation for which it is possible to find suitable mutation and crossover operators. These operators must be able to perform the genetic operation quickly and efficiently, and it is beneficial if they produce a valid solution. Moreover, the mutation of a genome or the combination of two genomes must lead to a solution that still sustains some properties of the original genome(s). Last but not least, it must be possible to determine a fitness value for all genomes.

For our problem, we choose a list representation. This is illustrated in Fig. 5. The list contains references to the mobile terminals along with the colors $\mathbf{C}_i$ that were assigned during the outer optimization in the central coordinator. The order of the mobile terminals in the list determines the assignment of resources to each mobile terminal. To assign resources, a placement algorithm traverses the list and assigns the first possible and free resource partition to the mobile terminals. The resource partitions must not yet be occupied, and the assignment must not be in conflict with the inner interference graph. For example, in Fig. 5, there is a conflict between mobile m_1 and m_{13} in the inner interference graph (i.e., $e_{1,13} = 1$), which is why m_1 cannot be assigned to $c_{0,1}$.

The list must contain at least as many entries as there are resources available in all three sectors together. However, the list may contain more entries, which will make it easier to fill up gaps with less problematic mobile terminals. This will increase the resource utilization.

The placement algorithm immediately takes care that constraints (9), (11), and (12) are fulfilled. In contrast, constraint (10) is taken into account during the subsequent evaluation of the genome by counting the number n_u of mobile terminals that have not been assigned resources. The second important factor during the evaluation is the number n_o

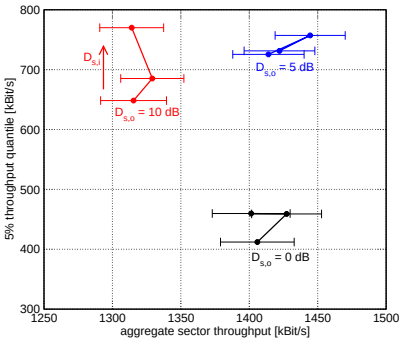

Fig. 6: Monte-Carlo Runs: Influence of desired SIR

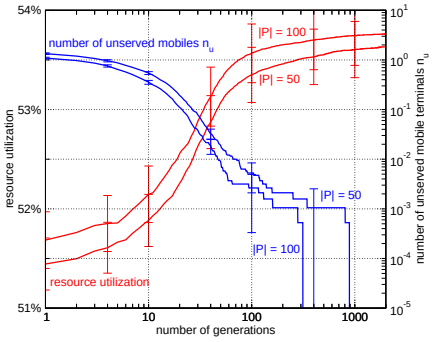

Fig. 7: Monte-Carlo Runs: Convergence of algorithm

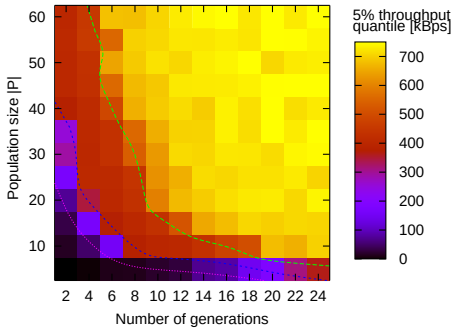

Fig. 8: Monte-Carlo Runs: Tradeoff between complexity and solution quality

of occupied resource partitions (i.e., the resource utilization). Finally, we set $u_i = 1$ for all mobiles m_i. Hence, the number of scheduled mobile terminals will be maximized, i.e., it will be attempted to schedule a mobile terminal in every resource partition. The overall fitness of a genome is then calculated as:

$$Fitness = n_o - n_u \quad . \tag{13}$$

C. Genetic algorithm and operators

We apply a steady state GA, which uses overlapping populations. When moving from one generation to the next, 50% of the population are replaced by the genetic operators. The applied mutator is a *swap mutator*, which swaps elements of the genome list with randomly chosen other elements with mutation probability p_{mut}. Furthermore, a *partial match crossover* is used, which is a standard crossover operator. It randomly selects an matching region in both parent genomes and swaps the content of these matching regions. Further genes are exchanged in order to not alter the number of occurences of a particular gene in the childs.

VI. Performance Evaluation

A. 802.16e scenario and simulation model

We consider an 802.16e-system [11] with a system bandwidth of 10 MHz and a MAC-frame-length of 5 ms. We assume the AMC zone to consist of 9 OFDM-symbols, corresponding to a total number of $48 \cdot 3$ available subchannels. AMC was applied ranging from QPSK 1/2 up to 64QAM 3/4. This results in a theoretical maximum raw data rate of about 6.2 Mbps within the AMC zone. The burst profile management is based on the exponential average of the SINR conditions of the terminal's previous data receptions.

The system model was implemented as a frame-level simulator using the event-driven simulation library IKR SimLib [13]. The path loss was modeled according to [14], terrain category B. Slow fading was considered using log-normal shadowing with standard deviation 8 dB. Frame errors were modeled based on BLER-curves obtained from physical layer simulations. The simulation model comprised all relevant protocols, such as fragmentation, ARQ and HARQ with chase combining. All results were obtained for the downlink direction with greedy traffic sources. Throughput measurements were done on the IP-layer, capturing all effects of SINR-variations, retransmissions, and MAC overhead.

We consider two scenarios. In the *static scenario*, $N = 9$ terminals are randomly placed in each cell sector. With this scenario, Monte-Carlo-like simulations are performed, where all terminals are randomly replaced for every drop. The drops have a duration of 4 s. Longer drop durations do not change the results significantly. In the *mobile scenario*, each cell sector contains $N = 9$ fully mobile terminals moving at a velocity of 30 km/h, which are restricted to their respective cell sector (see [10]). The Monte-Carlo runs were used to explore the parameter space, since they are much faster to perform, whereas a fully time-continuous simulation was performed in the mobile scenario to achieve final performance values.

The considered throughput performance metrics are the aggregate system throughput, which is proportional to the overall spectral efficiency, and the 5% quantile of the individual throughputs of all terminals, which correlates with the throughput of terminals close to the cell edge [15]. Hence, the 5% quantile is a very good fairness indicator.

B. Parameter choice

A large number of parameters influences the performance of the distributed interference coordination scheme. These parameters can be classified into two categories. The first category represents all parameters specific to the solution approach for the optimization problem. In our case, these are parameters inherent to the genetic algorithm, such as mutation rate or population size. In the following, we only consider the number of generations N_{gen} and the population size $|P|$. All other parameters were optimized by separate simulation runs.

The second category represents parameters which are specific to the general optimization problem. This includes the desired minimum SIR $D_{S,i}$ and $D_{S,o}$, or the coordination diameter d_{ic}. d_{ic} was set to 2, thus covering the full scenario. The influence of $D_{S,i}$ and $D_{S,o}$ is plotted in Fig. 6. An increase of the desired outer SIR $D_{S,o}$ leads to a better SIR at the cell edge and thus increases the 5% throughput quantile. Further increasing $D_{S,o}$ decreases the resource utilization, which counteracts the SIR improvement and eventually decreases the aggregate throughput performance.

The convergence behavior is shown in Fig. 7. Plotted is the overall resource utilization and the average number of unserved terminals after a certain number of generations N_{gen}. A higher resource utilization leads to a larger aggregate

throughput, while the number of unserved terminals affects the fairness. In particular, terminals in unfavorable positions at the cell edge will most likely be unserved for small N_{gen}, thus decreasing the cell edge performance. From Fig. 7 we can see that as few as $N_{gen} = 10$ generations bring the number of unserved terminals below one. For $N_{gen} = 100$, the algorithm already comes close to its optimum performance. The graph also shows that the aggregate throughput, which is mainly determined by the resource utilization, depends much less on the number of generations than the cell edge throughput. This also holds for the population size $|P|$.

C. Convergence and Complexity

The computational complexity is mainly determined by the number of generations N_{gen} and the population size $|P|$. Precisely, it is proportional to $N_{gen} \cdot |P|$. It is therefore of great interest to choose N_{gen} and $|P|$ such that the quality of the solution is maximized for a given computational effort. Figure 8 plots the 5% throughput quantile depending on N_{gen} and $|P|$. The chart shows that it is not beneficial to increase either N_{gen} or $|P|$. Instead, the best performance for a particular computational effort can be achieved for $|P| \approx 2N_{gen}$. Figure 8 further shows that it requires only a small computational effort to achieve near optimal results.

D. Comparison with existing IFCO schemes

Figure 9 compares the performance of the proposed distributed coordination scheme with an uncoordinated frequency reuse 3 system (also with beamforming antennas), and a system with fractional frequency reuse, which is locally coordinated based on local state information in every basestation (see [4]). Furthermore, the chart contains reference curves with global coordination according to [10] and [9]. All results of this figure were obtained in the mobile scenario with only $N_{gen} = 20$ generations.

The performance of the proposed distributed IFCO scheme is plotted for different values of $t_{\mathrm{C,up}}$ and $t_{\mathrm{C,delay}}$. The results show a big performance increase compared to the reference

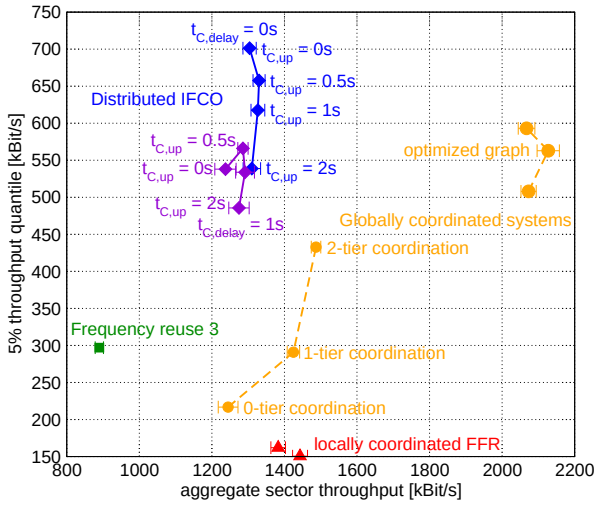

Fig. 9: Mobile scenario: Compariosn with other IFCO-schemes. Performance increase for $t_{C,delay} = 1$s when going from $t_{C,up} = 0$s to 0.5s is due to effects of burst profile management (see [9]).

frequency reuse 3 system, and the cell edge performance compared to a locally coordinated FFR system is greatly increased. Even for update periods and delays in the order of seconds the IFCO schemes achieves a large performance gain. Note also that in a nomadic scenario, which is a realistic use case for 802.16e networks, the performance gain will be mostly independent of $t_{\mathrm{C,up}}$ and $t_{\mathrm{C,delay}}$, hence the performance gains will even be larger compared to the mobile scenario when $t_{\mathrm{C,up}}$ and $t_{\mathrm{C,delay}}$ are in the order of seconds. This makes our distributed approach with a central mediator highly interesting compared to purely decentralized or local schemes, which have an inferior cell edge performance.

VII. Conclusion

We presented a distributed interference coordination algorithm for cellular OFDMA networks. The coordination was achieved by separating the initial global optimization problem into two separate problems, namely the inner and the outer optimization problem. We presented efficient approaches to solve these problems based on graph coloring heuristics and genetic algorithms. The complexity is well manageable, since the genetic algorithm converges after very few generations, allowing for efficient hardware-based real-time implementations. We evaluated the performance in a fully mobile scenario. The proposed scheme outperforms a reference reuse 3 system by more than 30% with respect to the aggregate spectral efficiency, and by more than 100% with respect to the cell edge throughput.

References

[1] 3GPP TSG RAN WG1#47bis R1-070040, "DL power allocation for dynamic interference avoidance in E-UTRA," 3rd Gen. Partnership Project, Sorrento, Italy, Tech. Rep., January 2007.

[2] 3GPP TSG RAN WG1#42 R1-050841, "Further analysis of soft frequency reuse scheme," 3rd Gen. Partnership Project, Tech. Rep., 2005.

[3] A. Simonsson, "Frequency reuse and intercell interference co-ordination in E-UTRA," in *Proc. IEEE VTC 2007-Spring*, Dublin, Ireland, April 2007, pp. 3091–3095.

[4] M. C. Necker, "Local interference coordination in cellular 802.16e networks," in *Proc. IEEE VTC 2007-Fall*, Baltimore, MA, Oct. 2007.

[5] W. Xiao, R. Ratasuk, A. Ghosh, R. Love, Y. Sun, and R. Nory, "Uplink power control, interference coordination and resource allocation for 3GPP E-UTRA," in *in Proc. IEEE VTC-2006*, 2006, pp. 1–5.

[6] S. G. Kiani, G. E. Oien, and D. Gesbert, "Maximizing multicell capacity using distributed power allocation and scheduling," in *Proc. IEEE WCNC 2007*, Kowloon, China, 2007, pp. 1690–1694.

[7] G. Li and H. Liu, "Downlink dynamic resource allocation for multi-cell OFDMA system," in *Proc. IEEE VTC 2003-Fall*, Orlando, FL, USA.

[8] M. C. Necker, "Integrated scheduling and interference coordination in cellular OFDMA networks," in *Proc. Broadnets*, Raleigh, NC, Sep. 2007.

[9] ——, "Coordinated fractional frequency reuse," in *Proc. ACM/IEEE MSWiM 2007*, Chania, Crete Island, October 2007.

[10] ——, "Towards frequency reuse 1 cellular FDM/TDM systems," in *Proc. ACM/IEEE MSWiM 2006*, Torremolinos, Spain, Oct. 2006, pp. 338–346.

[11] IEEE 802.16e, *IEEE Standard for Local and metropolitan area networks, Part 16: Air Interface for Fixed and Mobile Broadband Wireless Access Systems, Amendment 2: Physical and Medium Access Control Layers for Combined Fixed and Mobile Operation in Licensed Bands*, Feb. 2006.

[12] D. Brélaz, "New methods to color the vertices of a graph," *Communications of the ACM*, vol. 22, no. 4, pp. 251–256, April 1979.

[13] *IKR Simulation Library*. [Online]. Available: http://www.ikr.uni-stuttgart.de/Content/IKRSimLib/

[14] V. Erceg, L. Greenstein, S. Tjandra, S. Parkoff, A. Gupta, B. Kulic, A. Julius, and R. Bianchi, "An empirically based path loss model for wireless channels in suburban environments," *IEEE Journal on Selected Areas in Communications*, vol. 17, no. 7, pp. 1205–1211, July 1999.

[15] 3GPP TS25.814, *Physical layer aspects for evolved Universal Terrestrial Radio Access (UTRA) (Rel. 7)*, 3rd Gen. Partnership Project, June 2006.